Ultrasound-promoted chiral fluorescent organogel†

Yabing He, Zheng Bian,* Chuanqing Kang, Rizhe Jin and Lianxun Gao*

Received (in Montpellier, France) 7th May 2009, Accepted 16th June 2009
First published as an Advance Article on the web 30th July 2009
DOI: 10.1039/b909127k

In this paper, we have described a chiral binaphthyl-based fluorescent organogel. Very interestingly, similar to sonocrystallisation of organics, ultrasound can promote the gelation while it cannot occur spontaneously at relatively high temperature or low concentration. The fluorescence enhancement of the gel obtained *via* ultrasound irradiation is observed. In solution there exist rapid dynamic equilibria between (*S*)-**1** oligomers. The association interactions both between gelator molecules and between solvent and gelator molecules could together effect the helical growth of distorted (*S*)-**1** nanocrystals. The dihedral angle between the two naphthyl rings of the 1,1′-binaphthyl unit in (*S*)-**1** will increase upon gelation. It has been assumed that ultrasound can play an important role in gelation with a high energy barrier. Sonication-induced gelation is a rapid crystallisation behavior yielding fiber-like aggregates in a metastable system.

Introduction

In the past several years, ultrasound-induced gelation has received much interest from chemists.[1–6] In general, ultrasound is used to disrupt weak intermolecular interactions, which seems to be incompatible with the formation of an organogel. However, it also could offer the chance to mould new molecular shapes or to recombine molecular aggregates. Naota and Koori first proposed that ultrasound could change the conformations of gelator molecules to favor their polymerisation.[1] This is supported by the observations of Yi and Huang *et al.* for a family of cholesterol-based gelators.[2a] Furthermore, Naota *et al.* have assumed that ultrasound could destroy intramolecular H-bonding of metalated peptides and consequently that polymerisation by intermolecular H-bonding is initiated in the semistable system.[3] It has also been reported that ultrasound can promote gelation by partial destruction of H-bonding in the bulk[4] or a breaking–reorganisation of coordination bonds.[5] Recently, Bardelang *et al.* found that ultrasound may reshape sheet-like dipeptide particles into elongated molecular assemblies and that sonocrystallisation is at the origin of gelation.[6]

Nevertheless, there are still some questions to puzzle us since the ultrasonic effect is always unpredictable. For example, how does the acoustic field transmit its energy to the relevant molecular system? What are the common characteristics of ultrasound-induced gelation? And under what conditions can the ultrasonic effect be observed?

In the course of systematic syntheses of difunctional ligands based on chiral binaphthyl, we were surprised to discover the gelation ability of (*S*)-**1** (Scheme 1). In particular, ultrasound can promote gel formation at relatively high temperature or low concentration. We first observe that the ultrasound-induced gelation is a rapid crystallisation behavior similar to sonocrystallisation of organics.[7] Here we present our results of the gelation and corresponding analyses.

Results and discussion

Gel test

At first, attempts to recrystallise (*S*)-**1** from ethyl acetate in an icebox result in the formation of a partial gel. Subsequently, the gelation ability of (*S*)-**1** was evaluated in other solvents (see ESI†). In particular, although no gel is formed at room

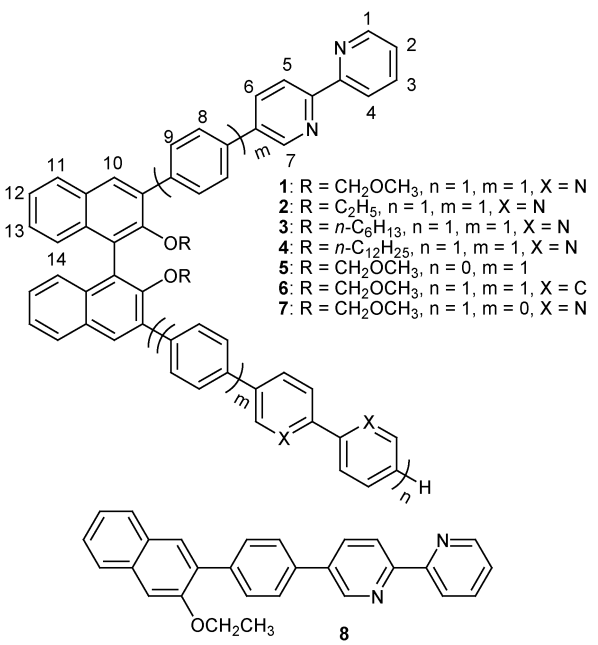

Scheme 1

State Key Laboratory of Polymer Physics and Chemistry, Changchun Institute of Applied Chemistry, Chinese Academy of Sciences, Graduate School of Chinese Academy of Sciences, Changchun, 130022, China.
E-mail: bianzh@ciac.jl.cn, lxgao@ciac.jl.cn;
Fax: +86 431 85697831; Tel: +86 431 85262265

† Electronic supplementary information (ESI) available: Gel tests, UV, PL, SEM, MS, NMR. CCDC reference numbers 664579, 709732 and 709733. For ESI and crystallographic data in CIF or other electronic format see DOI: 10.1039/b909127k

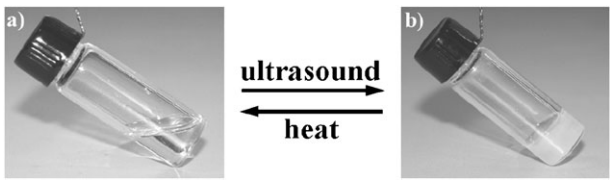

Fig. 1 Reversible gelation of a 3.4×10^{-2} M solution of (*S*)-**1** in toluene at 298 K. (a) Solution before sonication. (b) Gel just after sonication (0.26 W cm^{-2}, 40.0 kHz, 30 s).

temperature in toluene, xylene, mesitylene or ethylbenzene, short-time ultrasound irradiation (0.26 W cm^{-2}, 40.0 kHz, 60 s) can turn colorless solutions of 5 wt% into translucent gels (Fig. 1). However, the partial gels can spontaneously appear when aromatic solutions are allowed to stand at −10 °C for at least 6 h or the concentrations are increased to 10 wt% at room temperature. Furthermore, the gelation does not occur in 2.5 wt% ethyl acetate or acetone solution at room temperature, but ultrasound can induce it. The gelation experiments show that the sol–gel transition without sonication requires lower temperature, higher concentration and longer time. The gels formed *via* ultrasound are stable at room temperature and readily converted to the original solutions upon heating and then cooling.

The effects of cations on gel

Considering the chelating ability towards transition metal cations of the 2,2′-bipyridine units in (*S*)-**1**, the effect of cations on gel formation and stability is assessed. One equivalent of aqueous $FeSO_4 \cdot 7H_2O$ solution is added at the top of a toluene gel sample. No change is observed after 48 h except a slight modification of the interface between the gel phase and the aqueous phase. When the system is heated above 60 °C, the gel is destroyed, leading to a mixing and inversion of the toluene and water phases. On the other hand, the addition of one equivalent of $AgCF_3SO_3$ to (*S*)-**1** in toluene prevents the formation of a gel. Introduction of diluted HCl aqueous solution to the surface of preformed (*S*)-**1** toluene gel results in the gradual collapse of the gel within 30 min, due to the decomposition of the methoxymethyl (MOM) sidechains under the acid conditions as confirmed by the mass spectrum.

Absorption and emission spectra

The maximum absorption and emission wavelengths of (*S*)-**1** in dilute dichloromethane solution at room temperature are 312 nm and 390 nm, respectively (Fig. 2). Owing to the high critical gel concentration and the high molar absorption coefficient (ε, 104 400 M^{-1} cm^{-1} in toluene) of (*S*)-**1**, it is difficult to observe the change in the UV-vis spectrum of (*S*)-**1** in the gelation.

The fluorescence intensity of (*S*)-**1** in toluene first increases and then decreases with increasing concentration. The latter is typical of aggregation quenching. Furthermore, fluorescence enhancement of the gel obtained *via* ultrasound irradiation is observed, as a result of suppression of molecular freedom.[8] As shown in Fig. 3, the intensity of the maximal peak of (*S*)-**1** is enhanced drastically and then remains almost unchanged

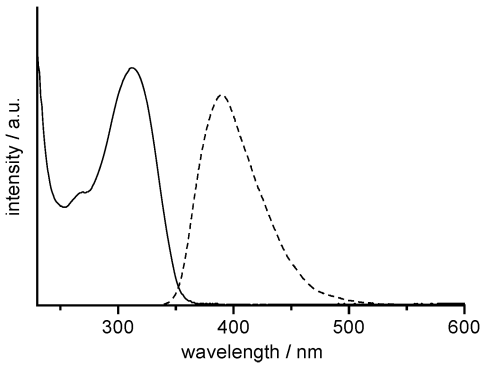

Fig. 2 Absorption (solid line) and emission (dashed line) spectra of (*S*)-**1** in CH_2Cl_2 (2.5×10^{-6} M) at room temperature. Excitation wavelength λ_{ex} = 320 nm.

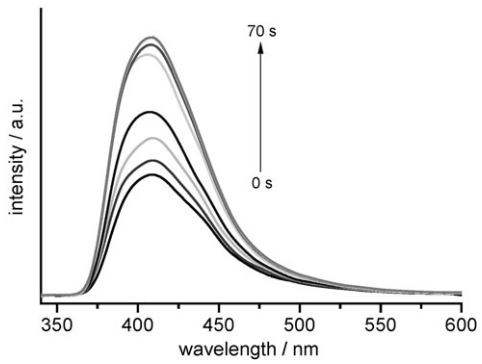

Fig. 3 Fluorescence spectra of (*S*)-**1** (5 wt%) in toluene at room temperature after different sonication times (0, 10, 20, 30, 40, 50, 60 and 70 s). Excitation wavelength λ_{ex} = 320 nm.

with prolonged irradiation, indicating gelation occurs upon ultrasonication.

Microscopic observation

Investigation of the micromorphology of (*S*)-**1** gel through transmission electron microscopy (TEM) has consistently revealed a well-developed network structure composed of fibrous aggregates. As shown in Fig. 4, the length of the fibers is more than several micrometres and the diameters are 8–15 nm in ethyl acetate, 17–40 nm in toluene, 17–52 nm in xylene and 13–38 nm in mesitylene, respectively, which is consistent with their transparency. Fibers featuring right-handed helicity are observed in toluene and mesitylene, independent of the cooling rate. When (*R*)-**1** is used instead, nanofibers with the opposite helicity are formed in toluene (Fig. 5). The scanning electron microscopic (SEM) images of the xerogel also show a predominant presence of three-dimensional entangling fiber-like aggregates, responsible for the observed gelation.

The influence of structural variation on gelation

The influence of structural variation on gelation is investigated. Racemic **1** has very poor solubility in toluene and does not gelate any solvent, indicating that homochirality is necessary for the gelation. When hydrophilic methoxymethyl (MOM) sidechains in (*S*)-**1** are replaced by hydrophobic ethyl,

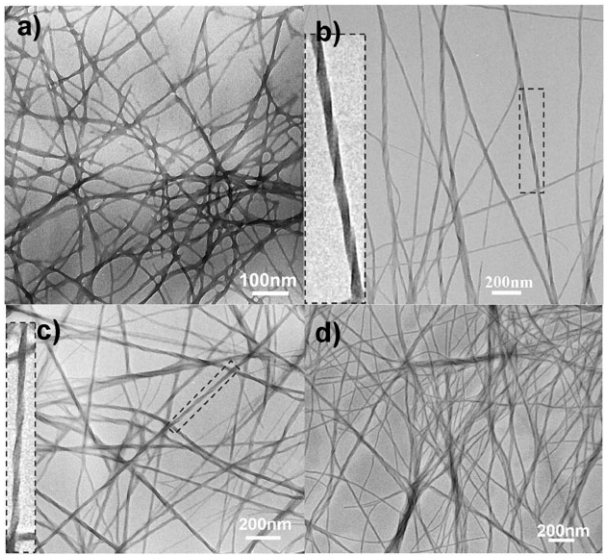

Fig. 4 TEM images of (*S*)-**1** gels obtained from ethyl acetate (a), toluene (b), mesitylene (c) and xylene (d). The inset shows the right-handed helical structure. The fibers on the TEM grids do not exhibit electron diffraction (ED).

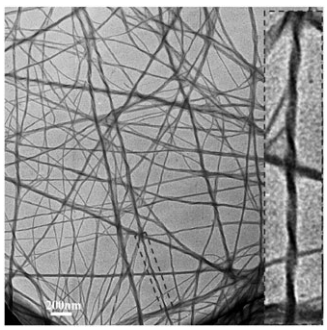

Fig. 5 TEM image of (*R*)-**1** gel from toluene. The inset shows the left-handed helical structure.

hexyl or dodecyl groups, it loses gelation power, implying that MOMs are indispensable in stabilising gelation through the lyophilic–lyophobic balance between solvent and gelator molecules. The fact that (*S*)-**5–7** do not possess gelation ability suggests that two phenylbipyridyl (PBP) segments are fundamental units of the gelator. Most probably, the combination of inherent properties, including homochirality, hydrophilic MOMs and suitable pendant aryls, drives the gelation.

Solution behaviors

To investigate the nature of aggregation and gelation, the solution behavior of (*S*)-**1** was explored. The ^{1}H NMR spectrum of (*S*)-**1** in $CDCl_3$ has shown concentration dependence at 298 K. The signals assigned to bipyridyl moieties shift upfield with increasing concentration, as a result of multi-molecular aggregation. However, no similar effect is observed in [D_8]toluene in the measured concentration range, possibly due to the fully aromatic gelator–solvent system. Furthermore, two dimensional nuclear Overhauser enhancement spectroscopy (2D NOESY) experiments in [D_8]toluene with

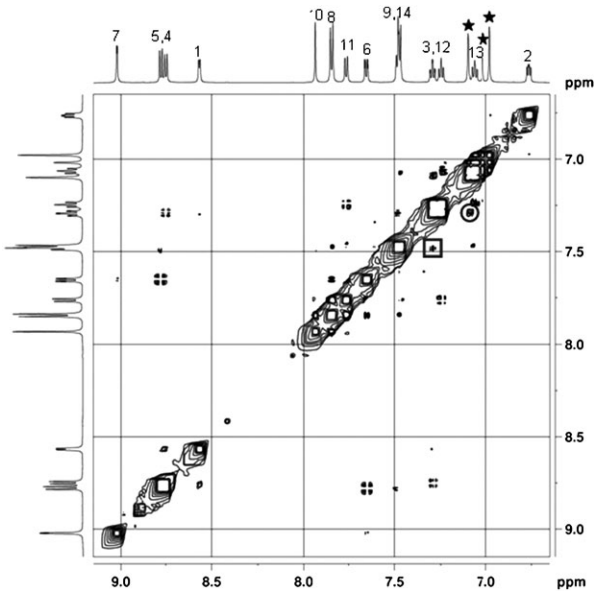

Fig. 6 2D NOESY spectra of (*S*)-**1** in [D_8]toluene with mixing time 500 ms. The dipole–dipole interactions between H3 and H9 of (*S*)-**1**s (squares) and between H3 of (*S*)-**1**s and the protons of undeuterated toluene molecules (circles). The signal peaks of toluene are marked "★".

mixing times ranging from 80 ms to 1100 ms explicitly show dipole–dipole interactions between H3 and H9 of (*S*)-**1**s (Fig. 6). This is also supported by the result of variable temperature NMR experiments on (*S*)-**1**. The chemical shifts of H3 and H9 evidently shift downfield upon increasing the temperature, indicative of the reduction of intermolecular π–π interactions. The dipole–dipole interaction could be due to the antiparallel π–π packing between two PBP units, in accordance with the centrosymmetric dimer structure of model compound **8** (Fig. 7). Here it should be mentioned that the 2D NOESY spectra also show the dipole–dipole interaction between H3 of (*S*)-**1** and the protons of undeuterated toluene, suggesting a strong association between toluene and (*S*)-**1**. The preservation of the C_2-symmetry of (*S*)-**1** on the NMR time scale, combined with observation of the electrospray mass spectrum, suggests that there exist rapid dynamic equilibria between oligomeric aggregates of (*S*)-**1** in solution.

DSC analyses

The DSC curves of the xerogels prepared from (*S*)-**1** toluene gel exhibit glass transitions in the range of 105–118 °C, and subsequent cold crystallisation and melting transitions (Fig. 8). In comparison, the DSC diagram of as-synthesised solid (*S*)-**1** only exhibits a melting transition. The glass transition is characteristic of the supramolecular aggregates.

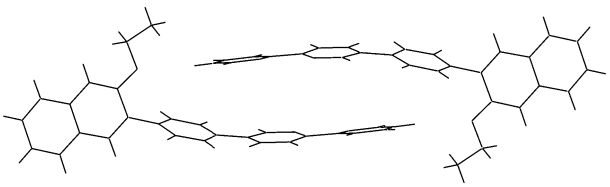

Fig. 7 The dimer structure of model compound **8**.

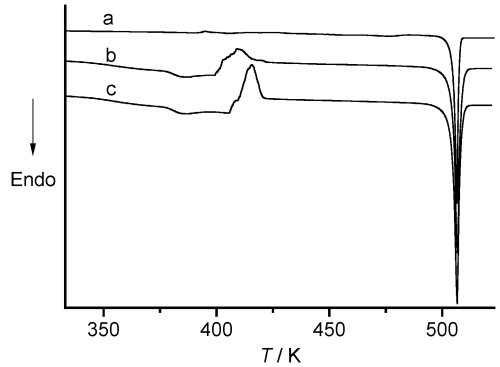

Fig. 8 DSC profile of (*S*)-**1**: the as-synthesised solid (a), and xerogels after sonication (0.26 W cm^{-2}, 40.0 kHz) for 20 s (b) and 40 s (c).

The melting transition of (*S*)-**1** xerogel is almost identical to that of as-synthesised (*S*)-**1**, suggesting that the accumulation structure of (*S*)-**1** after cold crystallisation is transformed into that of as-synthesised (*S*)-**1**.

On repeating the heating and cooling cycle, the glass transition temperature and cold crystallisation temperature are elevated and the transition ranges become broad, and finally the two transitions completely vanish, while the exothermic transition temperature when cooling is increased and the transition range becomes narrow (Fig. 9). It has been found by NMR that there exist toluene molecules in the original xerogel ((*S*)-**1**/toluene = 3/2, molar ratio), and after each heating and cooling cycle toluene can be partially removed until its complete disappearance. The explanations for these phenomena are rationalised as follows: (a) (*S*)-**1** and toluene are two necessary components of gel fibers and the structure of (*S*)-**1** gel fibers cannot exist without toluene; (b) the association between (*S*)-**1** and toluene could be destroyed before the melting transition, consequently causing the cold crystallisation; (c) supramolecular aggregates with different molar ratios of toluene and (*S*)-**1** have different thermal properties.

The gel structure

Deep insights into the gel structure are derived from X-ray diffraction (XRD) analyses. Attempts to obtain single crystals of (*S*)-**1** fail. However, high-quality single crystals of the analogue (*S*)-**2** can be acquired by slow evaporation of a chloroform–acetonitrile solution at room temperature. In

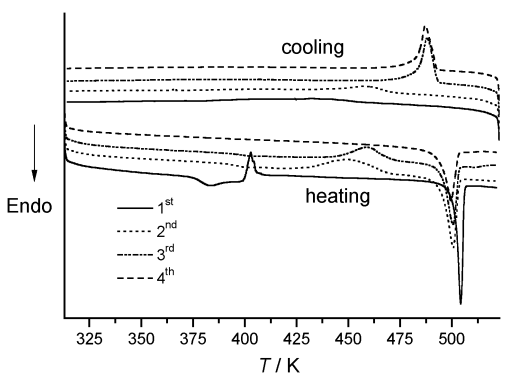

Fig. 9 DSC profile of four heating and cooling cycles of (*S*)-**1** xerogel.

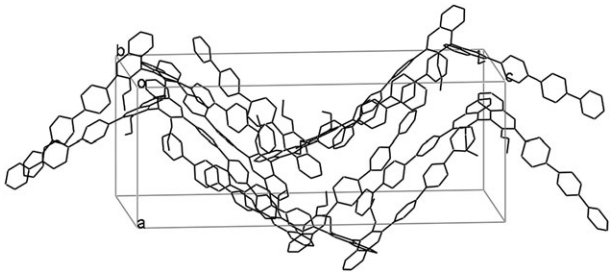

Fig. 10 The brick-wall type arrangement of (*S*)-**2**. The hydrogen atoms are omitted for the clarity. The parameters of (*S*)-**2** crystal: space group $P2_12_12_1$, a = 13.0290(18) Å, b = 19.014(3) Å, c = 34.024(5) Å, $\alpha = \beta = \gamma = 90.00°$.†

crystalline (*S*)-**2**, the electrostatic potential of opposite signs between PBP segments assists the aggregation of the molecules in a brick-wall type arrangement in which each molecule interacts with nearly two halves of neighboring molecules (Fig. 10). Moreover, the powder XRD pattern of (*S*)-**1** xerogels[9] from toluene (Fig. 11) exhibits some crystallisation peaks very close to those of crystalline (*S*)-**2**, suggesting that the accumulation structure of (*S*)-**1** gel fibers is very similar to that of crystalline (*S*)-**2**. The moderately broad peak shape means that the dimensions of the crystal are very small and there exists a lattice distortion in the fibers.[10] According to the above-mentioned NMR and DSC analyses, the lattice distortion could derive from the association between (*S*)-**1** and toluene molecules. The gel fibers could be formed by the helical growth of distorted nanocrystals along the *c* axis. The associations both between (*S*)-**1** molecules and between (*S*)-**1** and toluene could together effect the growth process. In comparison with tubular fibers described by Würthner *et al.*,[11] the diameter of (*S*)-**1** gel fibers is thicker, and the helical pitch is longer. The absolute configuration of gelator molecules subtly relates to the helicity of fibers.

The mechanism of ultrasound-induced gelation

Furthermore, the conformational movement of (*S*)-**1** in the gelation is deduced. The dihedral angle θ between the two naphthyl rings of 1,1′-binaphthyl derivatives with alkoxyl substituents at the 2,2′-positions is generally considered to be less than 90°.[12] Indeed, the θ values of (*S*)-**4** in crystal are 75.12°, 74.80° and 79.58° (Fig. 12, upper). The dihedral angle of (*S*)-**1** in solution could be close to those of (*S*)-**4**. However,

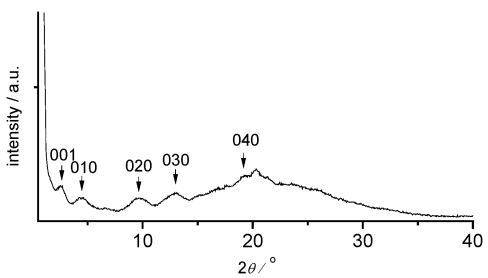

Fig. 11 The powder X-ray diffraction diagram of a xerogel prepared from (*S*)-**1** toluene gel. The extremely broad but high intensity band around 20° in 2θ implies the presence of a large number of π–π stacking interactions.

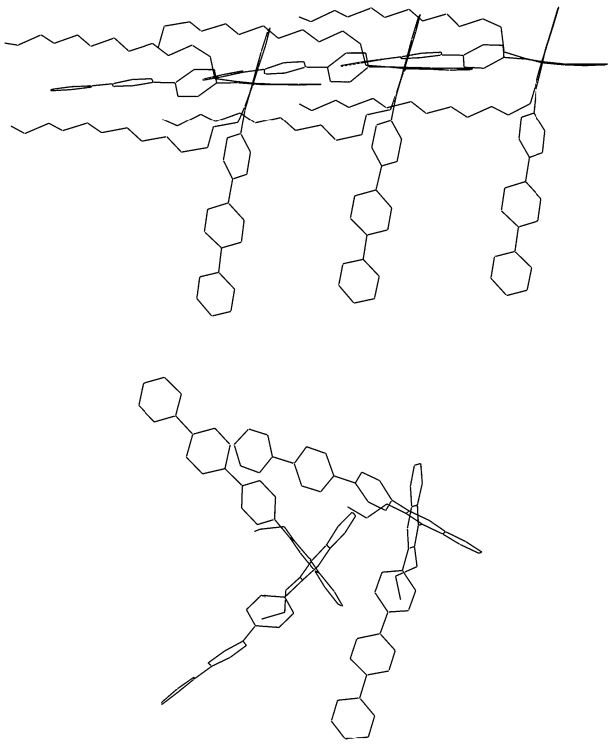

Fig. 12 *cis*-Conformation of 1,1′-binaphthyl in crystalline (*S*)-**4** (upper) and *trans*-conformation of 1,1′-binaphthyl in crystalline (*S*)-**2** (lower). The hydrogen atoms are omitted for clarity.

the θ values of (*S*)-**2** in the crystal are 105.86° and 115.83° (Fig. 12, lower), suggesting that the *trans*-conformation of 1,1′-binaphthyl is advantageous in the gel fiber with the brick-wall structure. Accordingly, the conclusion may be drawn that the dihedral angle of (*S*)-**1** will increase on gelation. The enlargement of the dihedral angle is favorable for the formation of a fiber structure with a high aspect ratio.

However, such an enlargement of the dihedral angle will increase the molecular potential energy.[13] Interestingly, all the previously reported ultrasound-induced gelations have to pass through a process with quite a high energy barrier, such as the formation of a conformation with higher potential energy,[1,2] partial destruction of H-bonding,[4] breaking–reorganisation of H-bonding[3] or coordination bonds,[5] or the modification of morphology of the material.[6] So a high energy barrier could be a requirement for ultrasound-induced gelation. In our case, the high energy barrier for gelation arises from the formation of a large dihedral angle and the conformational restriction within the gel fibers.

The supersaturation of a solution of (*S*)-**1** at low temperature can drive the gelation. Then why does ultrasound promote the gelation while it cannot spontaneously occur at relatively high temperatures or low concentrations? The characteristics of the gelation described here are very similar to the sono-crystallisation behavior of organics.[7] Acoustically induced cavitation is particularly effective at inducing the crystal nucleation of organics. Under sonication, the width of the metastable zone of the supersaturated solution is reduced and nucleation starts at a low level of supersaturation.[7] Considering that the gelation is a partial crystallisation behavior,[14] we can well understand the ultrasonic effect. The cavitation or shock wave caused by ultrasound irradiation[15] may cause the mechano-sensitive dihedral angle of (*S*)-**1** to enlarge. The nucleation and growth of crystalline (*S*)-**1** fibers can also occur more easily.

Conclusion

In conclusion, we have described a chiral binaphthyl-based fluorescent organogel. Like sonocrystallisation of organics, ultrasound can promote the gelation at relatively high temperatures or low concentrations. The gel fibers could be formed by the helical growth of distorted nanocrystals containing solvent and gelator molecules. The dihedral angle of (*S*)-**1** will increase on gelation. Ultrasound is suitable for stimulating gelation with a high energy barrier. Sonication-induced gelation is a rapid crystallisation behavior to give fiber-like aggregates in a metastable system. The gelator molecule contains two rigid π-conjugated segments with simple MOM substituents and without long alkyl chains, which endows the gel system with better potential for optoelectronic applications. This work also demonstrates the potential of the supramolecular binding motif between bipyridylphenyl units. 2,2′-Bipyridine finds use not only as a ligand for transition metal ions.

Experimental

Materials

All reagents and solvents are obtained from commercial supplies and used directly without further purification unless otherwise stated. The solvents for spectroscopic studies are purified according to standard methods.

Synthesis of the compounds investigated

(*S*)-3,3′-Bis(4-(2,2′-bipyridin-5-yl)phenyl)-2,2′-dimethoxymethoxy-1,1′-binaphthyl (*S*)-1. To a degassed solution of 5-(4-bromophenyl)-2,2′-bipyridine[16] (1.30 g, 4.18 mmol) in toluene (50 mL) is added $Pd(PPh_3)_4$ (120.7 mg, 0.10 mmol) under a nitrogen atmosphere. After the resulting mixture is stirred for 10 minutes at room temperature, 2,2′-bis(methoxymethoxy)-1,1′-binaphthyl-3,3′-diboronic acid pinacol ester (*S*)-**9**[17] (1.30 g, 2.09 mmol) and 1 M Na_2CO_3 (25 mL) are added sequentially into the mixture. Then the mixture is refluxed for 3 days under nitrogen. After removal of the solvent, the resulting residue is poured into water (100 mL) and extracted with CH_2Cl_2 (100 mL × 3). The combined organic layer is washed with brine (80 mL) and dried with anhydrous $MgSO_4$. Evaporation of the solvent gives a yellow residue which is purified by silica gel column chromatography (CH_2Cl_2 : EtOAc = 5 : 1 (v/v)) to afford pure (*S*)-**1** in 75% yield as an off-white powder. Mp 233–234 °C; $[\alpha]_D^{20}$ 269 (c = 0.1 in CH_2Cl_2); FT-IR (KBr, cm^{-1}): 752, 969, 997, 1150, 1159, 1459; ^1H NMR (400 MHz, $CDCl_3$) δ (ppm): 2.42 (s, 6H), 4.45 (d, 6.0 Hz, 2H), 4.51 (d, 6.0 Hz, 2H), 7.34 (m, 6H), 7.45 (m, 2H), 7.79 (d, 8.0 Hz, 4H), 7.84 (td, 7.6 Hz, 1.6 Hz, 2H), 7.94 (m, 6H), 8.03 (s, 2H), 8.11 (dd, 8.0 Hz, 2.0 Hz, 2H), 8.47 (d, 8.0 Hz, 2H), 8.52 (d, 8.0 Hz, 2H), 8.72 (d, 4.0 Hz, 2H), 9.02 (d, 1.6 Hz, 2H); ^{13}C NMR (100 MHz, $CDCl_3$)

δ (ppm): 155.83, 154.98, 151.29, 149.23, 147.56, 139.02, 136.94, 136.47, 136.01, 135.08, 134.68, 133.71, 130.87, 130.60, 130.35, 127.94, 126.95, 126.63, 126.52, 126.43, 125.32, 123.70, 121.06, 98.66, 55.94; MS (ESI) (m/z) calc. for $C_{56}H_{42}N_4O_4$: 834.9, Found: 835.4; Anal. calc. for $C_{56}H_{42}N_4O_4$: C, 80.55; H, 5.07; N, 6.71, Found: C, 80.69; H, 5.00; N, 6.69%.

A procedure similar to that used for (*S*)-**1** is used to prepare (*S*)-**2**–**7** and **8** (Fig. 13).

(*S*)-3,3′-Bis(4-(2,2′-bipyridin-5-yl)phenyl)-2,2′-diethoxy-1,1′-binaphthyl (*S*)-2. (*S*)-**2** is prepared from 5-(4-bromophenyl)-2,2′-bipyridine and 2,2′-diethyloxy-1,1′-binaphthyl-3,3′-diboronic acid pinacol ester (*S*)-**10**. Yield 72%; mp 235–236 °C; $[\alpha]_D^{20}$ 277 (c = 0.1 in CH_2Cl_2); FT-IR (KBr, cm^{-1}): 752, 1459; ^{1}H NMR (400 MHz, $CDCl_3$) δ (ppm): 0.68 (t, 8.0 Hz, 6H), 3.34 (m, 2H), 3.59 (m, 2H), 7.24–7.28 (m, 4H), 7.35 (t, 8.4 Hz, 2H), 7.43 (m, 2H), 7.78 (d, 8.4 Hz, 4H), 7.87 (t, 7.2 Hz, 2H), 7.93 (m, 6H), 8.03 (s, 2H), 8.13 (dd, 8.4 Hz, 2.0 Hz, 2H), 8.49 (d, 7.2 Hz, 2H), 8.53 (d, 8.0 Hz, 2H), 8.73 (d, 4.4 Hz, 2H), 9.03 (d, 1.6 Hz, 2H); ^{13}C NMR (100 MHz, $CDCl_3$) δ (ppm): 155.89, 154.91, 153.63, 149.22, 147.57, 139.27, 136.94, 136.31, 136.13, 135.06, 134.74, 133.88, 130.65, 130.16, 128.06, 126.77, 126.40, 126.32, 125.95, 124.92, 123.67, 121.08, 121.03, 68.95, 15.38; MS (ESI) (m/z) calc. for $C_{56}H_{42}N_4O_2$: 803.0, Found: 803.4; Anal. calc. for $C_{56}H_{42}N_4O_2$: C, 83.77; H, 5.27; N, 6.98, Found: C, 83.27; H, 5.31; N, 6.90%.

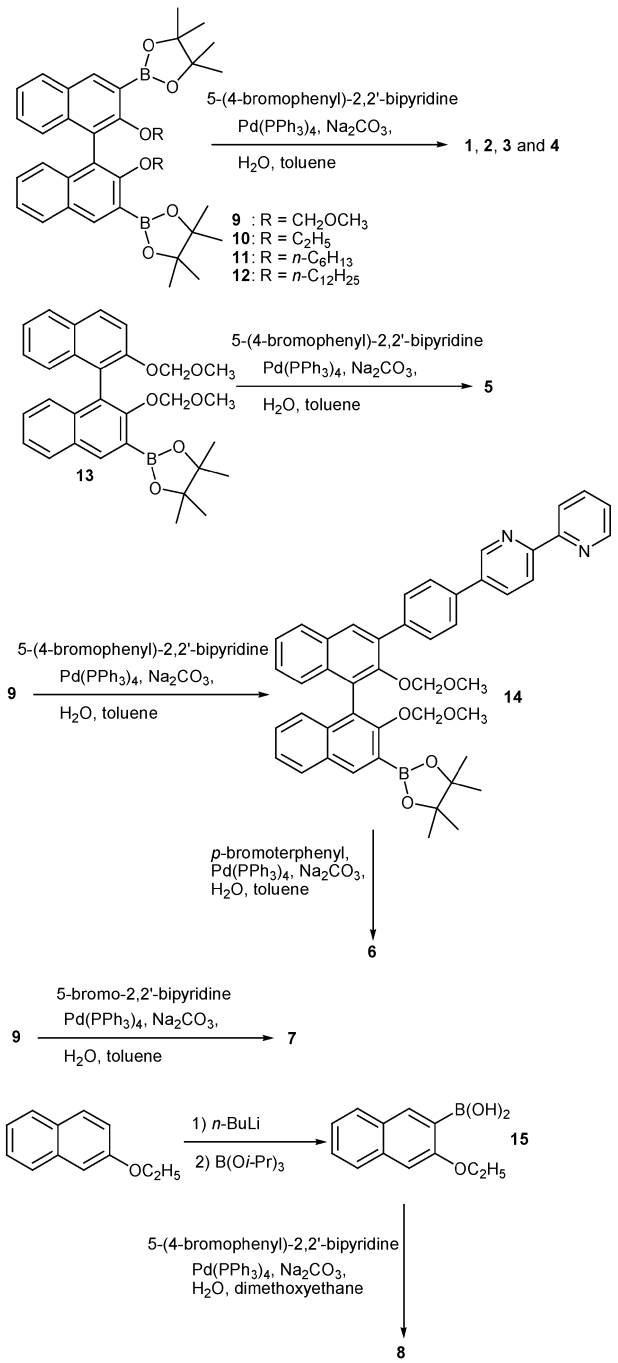

Fig. 13 Synthetic routes to **1**–**8**.

(*S*)-3,3′-Bis(4-(2,2′-bipyridin-5-yl)phenyl)-2,2′-dihexyloxy-1,1′-binaphthyl (*S*)-3. (*S*)-**3** is prepared from 5-(4-bromophenyl)-2,2′-bipyridine and 2,2′-dihexyloxy-1,1′-binaphthyl-3,3′-diboronic acid pinacol ester (*S*)-**11**. Yield 69%; mp 78–79 °C; $[\alpha]_D^{20}$ 261 (c = 0.1 in CH_2Cl_2); FT-IR (KBr, cm^{-1}): 751, 1459, 2855, 2925; ^{1}H NMR (400 MHz, $CDCl_3$) δ (ppm): 0.63–0.76 (m, 14H), 0.91–0.97 (m, 8H), 3.20 (m, 2H), 3.50 (m, 2H), 7.28 (d, 3.6 Hz, 4H), 7.33 (m, 2H), 7.43 (m, 2H), 7.77 (d, 8.4 Hz, 4H), 7.85 (td, 8.0 Hz, 1.6 Hz, 2H), 7.94 (m, 6H), 8.02 (s, 2H), 8.12 (dd, 8.0 Hz, 2.0 Hz, 2H), 8.47 (d, 8.0 Hz, 2H), 8.52 (d, 8.4 Hz, 2H), 8.72 (d, 4.8 Hz, 2H), 9.03 (d, 1.6 Hz, 2H); ^{13}C NMR (100 MHz, $CDCl_3$) δ (ppm): 155.92, 154.91, 153.65, 149.23, 147.58, 139.27, 136.95, 136.28, 136.18, 135.07, 134.75, 133.93, 130.75, 130.15, 128.06, 126.74, 126.44, 126.23, 126.00, 124.86, 123.68, 121.09, 121.04, 72.94, 31.14, 29.76, 25.09, 22.37, 13.90; MS (ESI) (m/z) calc. for $C_{64}H_{58}N_4O_2$: 915.2, Found: 915.6; Anal. calc. for $C_{64}H_{58}N_4O_2$: C, 83.99; H, 6.39; N, 6.12, Found: C, 83.87; H, 6.41; N, 6.17%.

(*S*)-3,3′-Bis(4-(2,2′-bipyridin-5-yl)phenyl)-2,2′-didodecyloxy-1,1′-binaphthyl (*S*)-4. (*S*)-**4** is prepared from 5-(4-bromophenyl)-2,2′-bipyridine and 2,2′-didodecyloxy-1,1′-binaphthyl-3,3′-diboronic acid pinacol ester (*S*)-**12**. Yield 70%; mp 121–122 °C; $[\alpha]_D^{20}$ 228 (c = 0.1 in CH_2Cl_2); FT-IR (KBr, cm^{-1}): 752, 1459, 2851, 2922; ^{1}H NMR (400 MHz, $CDCl_3$) δ (ppm): 0.74–1.24 (m, 46H), 3.20 (m, 2H), 3.50 (m, 2H), 7.28 (d, 3.6 Hz, 4H), 7.35 (m, 2H), 7.43 (m, 2H), 7.77 (d, 8.0 Hz, 4H), 7.87 (t, 7.6 Hz, 2H), 7.94 (m, 6H), 8.01 (s, 2H), 8.14 (dd, 8.4 Hz,1.6 Hz, 2H), 8.50 (d, 8.0 Hz, 2H), 8.55 (d, 8.0 Hz, 2H), 8.73 (d, 8.4 Hz, 2H), 9.03 (d, 1.6 Hz, 2H); ^{13}C NMR (100 MHz, $CDCl_3$) δ (ppm): 155.94, 154.93, 153.68, 149.22, 147.57, 139.25, 136.90, 136.28, 136.15, 135.00, 134.75, 133.93, 130.74, 130.15, 128.06, 126.72, 126.44, 126.22, 125.99, 124.85, 123.65, 121.06, 121.00, 72.94, 31.89, 29.83, 29.66, 29.61, 29.48, 29.35, 28.99, 25.44, 22.65, 14.06; MS (ESI) (m/z) calc. for $C_{76}H_{82}N_4O_2$: 1083.5, Found: 1083.8; Anal. calc. for $C_{76}H_{82}N_4O_2$: C, 84.25; H, 7.63; N, 5.17, Found: C, 84.17; H, 7.75; N, 5.22%.

(*S*)-3-(4-(2,2′-Bipyridin-5-yl)phenyl)-2,2′-dimethoxymethoxy-1,1′-binaphthyl (*S*)-5. (*S*)-**5** is prepared from 5-(4-bromophenyl)-2,2′-bipyridine and 2,2′-dimethoxymethoxy-1,1′-binaphthyl-3-boronic acid pinacol ester (*S*)-**13**.[17] Yield 73%; mp 118–119 °C; $[\alpha]_D^{20}$ −127 (c = 0.1 in CH_2Cl_2); FT-IR (KBr, cm^{-1}): 752, 989, 1016, 1036, 1150, 1243, 1460; ^{1}H NMR (400 MHz, $CDCl_3$) δ (ppm): 2.34 (s, 3H), 3.25 (s, 3H), 4.36 (d, 8.0 Hz, 1H), 4.42

(d, 8.0 Hz, 1H), 5.10 (d, 8.0 Hz, 1H), 5.20 (d, 8.0 Hz, 1H), 7.23–7.31 (m, 4H), 7.39 (m, 2H), 7.43 (m, 1H), 7.62 (d, 9.2 Hz, 1H), 7.77 (d, 8.0 Hz, 2H), 7.88 (m, 4H), 7.93 (d, 8.4 Hz, 1H), 7.97 (d, 9.2 Hz, 1H), 8.01 (s, 1H), 8.12 (d, 8.0 Hz, 1H), 8.51 (d, 7.2 Hz, 1H), 8.55 (d, 7.2 Hz, 1H), 8.73 (d, 4.0 Hz, 1H), 9.01 (s, 1H); ^{13}C NMR (100 MHz, $CDCl_3$) δ (ppm): 155.89, 154.97, 152.97, 151.00, 149.23, 147.56, 139.18, 136.93, 136.35, 136.07, 135.06, 134.84, 134.10, 133.50, 131.02, 130.43, 130.28, 129.72, 128.03, 127.82, 126.86, 126.55, 126.35, 125.95b, 125.79, 125.25, 124.12, 123.68, 121.09, 121.04, 116.77, 98.79, 95.14, 56.02, 55.93; MS (ESI) (m/z) calc. for $C_{40}H_{32}N_2O_4$: 604.7, Found: 605.4; Anal. calc. for $C_{40}H_{32}N_2O_4$: C, 79.45; H, 5.33; N, 4.63, Found: C, 79.37; H, 5.34; N, 4.70%.

(*S*)-3-(4-(2,2′-Bipyridin-5-yl)phenyl)-3′-(*p*-terphenyl)-2,2′-dimethoxymethoxy-1,1′-binaphthyl (*S*)-6. (*S*)-**6** is prepared by the sequential coupling of diboronic acid pinacol ester **9** and 5-(4-bromophenyl)-2,2′-bipyridine and *p*-bromoterphenyl[18] according to the procedure described in Fig. 13. Yield 35% (two steps); mp 218–219 °C; $[\alpha]_D^{20}$ 275 (c = 0.1 in CH_2Cl_2); FT-IR (KBr, cm^{-1}): 749, 965, 994, 1157, 1459; ^{1}H NMR (400 MHz, $CDCl_3$) δ (ppm): 2.40 (s, 3H), 2.42 (s, 3H), 4.45 (m, 2H), 4.49 (m, 2H), 7.31–7.50 (m, 10H), 7.66 (d, 7.2 Hz, 2H), 7.21 (d, 8.4 Hz, 2H), 7.76–7.80 (m, 6H), 7.88 (d, 8.0 Hz, 2H), 7.94 (m, 5H), 8.03 (d, 2.4 Hz, 2H), 8.17 (d, 6.4 Hz, 1H), 8.58 (br, 2H), 8.75 (d, 3.2 Hz, 1H), 9.04 (s, 1H); ^{13}C NMR (100 MHz, $CDCl_3$) δ (ppm): 155.80, 154.90, 151.45, 151.30, 149.19, 147.56, 140.69, 140.29, 139.60, 139.14, 138.13, 137.03, 136.46, 136.12, 135.15, 135.04, 134.73, 133.79, 133.67, 130.91, 130.58, 130.40, 130.08, 128.83, 127.94, 127.57, 127.39, 127.04, 126.96, 126.91, 126.75, 126.51, 126.43, 125.32, 125.27, 123.74, 121.15, 98.67, 55.97, 55.95; MS (ESI) (m/z) calc. for $C_{58}H_{44}N_2O_4$: 833.0, Found: 833.5; Anal. calc. for $C_{58}H_{44}N_2O_4$: C, 83.63; H, 5.32; N, 3.36, Found: C, 83.75; H, 5.43; N, 3.24%.

(*S*)-3,3′-Bis((2,2′-bipyridin)-5-yl)-2,2′-dimethoxymethoxy-1,1′-binaphthyl (*S*)-7. (*S*)-**7** is prepared from 5-bromo-2,2′-bipyridine[19] and 2,2′-dimethoxymethoxy-1,1′-binaphthyl-3,3′-di-boronic acid pinacol ester. Yield 78%; mp 152–154 °C; $[\alpha]_D^{20}$ 223 (c = 0.1 in CH_2Cl_2); FT-IR (KBr, cm^{-1}): 752, 926, 988, 1159, 1462; ^{1}H NMR (400 MHz, $CDCl_3$) δ (ppm): 2.45 (s, 6H), 4.43 (d, 8.0 Hz, 2H), 4.46 (d, 8.0 Hz, 2H), 7.34 (m, 6H), 7.48 (m, 2H), 7.86 (td, 8.0 Hz, 1.6 Hz, 2H), 7.95 (d, 8.0 Hz, 2H), 8.05 (s, 2H), 8.28 (dd, 8.4 Hz, 1.6 Hz, 2H), 8.50 (d, 8.0 Hz, 2H), 8.54 (d, 8.4 Hz, 2H), 8.72 (m, 2H), 9.07 (d, 1.6 Hz, 2H); ^{13}C NMR (100 MHz, $CDCl_3$) δ (ppm): 155.90, 154.82, 151.50, 149.61, 149.22, 137.96, 136.99, 134.80, 133.96, 131.97, 130.83, 130.76, 128.10, 126.95, 126.54, 126.38, 125.58, 123.76, 121.18, 120.48, 98.90, 56.17; MS (ESI) (m/z) calc. for $C_{44}H_{34}N_4O_4$: 682.3, Found: 682.1; Anal. calc. for $C_{44}H_{34}N_4O_4$: C, 77.40; H, 5.02; N, 8.21, Found: C, 77.90; H, 5.34; N, 8.30%.

5-(4-(3-Ethoxynaphthalen-2-yl)-phenyl)-2,2′-bipyridine 8. 8 is synthesised according to the procedures described in Fig. 13. 5-(4-Bromophenyl)-2,2′-bipyridine (2.06 g, 6.61 mmol) is dissolved in dimethoxyethane (80 mL) to give a colorless solution. The solution is purged with nitrogen for 15 minutes, then 3-ethyloxynaphthyl-2-boronic acid **15** (1.50 g, 6.94 mmol), $Pd(PPh_3)_4$ (0.20 mmol, 241.4 mg) and l M Na_2CO_3 (40 mL) are added sequentially into the solution under nitrogen. The resulting mixture is stirred for 72 h under reflux. After removal of the solvent, the residue is extracted with methylene chloride (100 mL × 4). The combined organic phase is washed with brine (100 mL) and dried with anhydrous $MgSO_4$. The solvent is removed by rotary evaporation to give an off-white solid. Chromatography on gel silica (petroleum ether–EtOAc–CH_2Cl_2 = 10/1/1 (v/v/v)), following by recrystallisation in ethyl acetate and *n*-hexane, yields colorless block crystal in 76% yield. Mp 146–148 °C; FT-IR (KBr, cm^{-1}): 746, 800, 1180, 1458; ^{1}H NMR (400 MHz, $CDCl_3$) δ (ppm): 1.46 (*t*, 8.0 Hz, 3H), 4.21 (q, 8.0 Hz, 2H), 7.25 (d, 4.0 Hz, 1H), 7.35 (m, 2H), 7.46 (*t*, 7.2 Hz, 1H), 7.72–7.87 (m, 8H), 8.11 (dd, 8.0 Hz, 2.0 Hz, 1H), 8.46 (d, 8.0 Hz, 1H), 8.50 (d, 8.4 Hz, 1H), 8.72 (d, 4.0 Hz, 1H), 9.01 (d, 1.6 Hz, 1H); ^{13}C NMR (100 MHz, $CDCl_3$) δ (ppm): 155.92, 154.83, 154.48, 149.22, 147.58, 138.53, 136.94, 136.27, 136.14, 135.12, 134.14, 131.66, 130.52, 129.97, 128.78, 127.74, 126.54, 126.42, 126.31,123.92, 123.66, 121.08, 121.03, 63.91, 14.64; MS (ESI) (m/z) calc. for $C_{28}H_{22}N_2O$: 402.5, Found: 403.1; Anal. calc.. for $C_{28}H_{22}N_2O$: C, 83.56; H, 5.51; N, 6.96, Found: C, 83.68; H, 5.72; N, 6.79%.

The gelation test method

A mixture of (*S*)-**1–7** (25 mg) and solvent (0.5 mL) is placed in a glass test tube (35 mm ×15 mm), which is capped and heated in an oil bath until the compound is dissolved in the solvent. After the solution is allowed to stand at room temperature (25 ± 5 °C) for 3 h, the state of the mixture is evaluated by the "stable to inversion of test tube" method. If the solution is stable at room temperature, the solution is allowed to stand at −10 °C for at least 6 h or the solution is sonicated for 60 seconds using a sonoreactor (0.26 W cm^{-1}, 40 kHz).

Measurements

^{1}H NMR and ^{13}C NMR spectra were recorded on a Bruker AV400 or AV600 spectrometer. Chemical shifts are reported downfield from TMS (δ = 0) for ^{1}H NMR. For ^{13}C NMR spectra, chemical shifts are reported on the scale relative to deuterated solvent as internal standard ($CDCl_3$, δ = 77.00). Coupling constants are reported in hertz. Mass spectra (ESI-MS) were recorded with a Thermo Finnigan LCQ instrument. IR spectra were performed on a Bio-Rad FTS135 infrared spectrometer with KBr pellets. Optical rotations were measured on a 341LC polarimeter. Elemental analyses (C, H, N) were carried out with a VarioEL instrument. Chromatographic purification was conducted using 100–200 mesh silica gel. UV-Vis spectra were recorded on a UV-2500 UV-vis spectrophotometer using a 1 cm cuvette. Solid-state UV-Vis spectra were obtained by drop-casting the solution onto a microscope slide. Fluorescent spectra were recorded on a Perkin-Elmer LS 50B fluorescence spectrophotometer at room temperature. TEM was performed on a JEOL JEM-1011 transmission electron microscope operated at an acceleration voltage of 100 kV. Samples were prepared by wiping a small amount of gel samples onto a carbon-coated copper grid followed by naturally evaporating the solvent. SEM pictures were taken using an XL 30 ESEM FEG field emission scanning electron microscope with 20 kV operating voltage.

PXRD patterns were recorded by PW1710 BASED X-ray diffractometer with CuKα1 radiation source. X-Ray crystallographic analysis was performed on a Bruker SMART APEX CCD diffractometer with graphite-monochromated Mo–Kα radiation (λ = 0.71073 Å) operated at 2.0 kW (50 kV, 40 mA).†

Acknowledgements

The work is supported by the National Natural Science Foundation of China (B020104) and the Free Exploration Project of Innovation III of Changchun Institute of Applied Chemistry (CX07QZJC-02).

Notes and references

1 T. Naota and H. Koori, *J. Am. Chem. Soc.*, 2005, **127**, 9324.
2 (*a*) J. Wu, T. Yi, T. Shu, M. Yu, Z. Zhou, M. Xu, Y. Zhou, H. Zhang, J. Han, F. Li and C. Huang, *Angew. Chem., Int. Ed.*, 2008, **47**, 1063; (*b*) C. Wang, D. Zhang and D. Zhu, *J. Am. Chem. Soc.*, 2005, **127**, 16372.
3 K. Isozaki, H. Takaya and T. Naota, *Angew. Chem., Int. Ed.*, 2007, **46**, 2855.
4 (*a*) K. M. Anderson, G. M. Day, M. J. Paterson, P. Byrne, N. Clarke and J. W. Steed, *Angew. Chem., Int. Ed.*, 2008, **47**, 1058; (*b*) Y. Li, T. Wang and M. Liu, *Tetrahedron*, 2007, **63**, 7468.
5 S. Zhang, S. Yang, J. Lan, Y. Tang, Y. Xue and J. You, *J. Am. Chem. Soc.*, 2009, **131**, 1689.
6 D. Bardelang, F. Camerel, J. C. Margeson, D. M. Leek, M. Schmutz, M. B. Zaman, K. Yu, D. V. Soldatov, R. Ziessel, C. I. Ratcliffe and J. A. Ripmeester, *J. Am. Chem. Soc.*, 2008, **130**, 3313.
7 (*a*) L. McCausland and P. Cains, *Chem. Ind.*, 2003, (5), 15; (*b*) N. Amara and B. Ratsimba, *Ultrason. Sonochem.*, 2001, **8**, 265; (*c*) L. McCausland, P. Cains and P. D. Martin, *Chem. Eng. Prog.*, 2001, **97**, 56; (*d*) E. Dalas, *J. Cryst. Growth*, 2001, **222**, 287; (*e*) L. H. Thompson and L. K. Doraiswamy, *Chem. Eng. Sci.*, 2000, **55**, 3085.
8 M. Asai, K. Sugiyasu, N. Fujita and S. Shinkai, *Chem. Lett.*, 2004, **33**, 120.
9 In contrast to the obervations of Yi and Huang *et al.* (see ref. 2), the powder XRD patterns of (*S*)-**1** xerogels prepared from spontaneously-formed and sonication-induced gels are almost identical, suggesting that their accumulation structures are similar.
10 L. E. Alexander, *X-Ray Diffraction Methods in Polymer Science*, Wiley Interscience, New York, 1969.
11 S. Yao, U. Beginn, T. Gress, M. Lysetska and F. Würthner, *J. Am. Chem. Soc.*, 2004, **126**, 8336.
12 L. Pu, *Chem. Rev.*, 1998, **98**, 2405.
13 S. Fujiyoshi, S. Takeuchi and T. Tahara, *J. Phys. Chem. A*, 2004, **108**, 5938.
14 P. Terech and R. G. Weiss, *Chem. Rev.*, 1997, **97**, 3133.
15 K. S. Suslick and L. A. Crum, in *Encyclopedia of Acoustics*, ed. M. J. Crocker, John Wiley & Sons, New York, 1997, pp. 271–282.
16 V. N. Kozhevnikov, D. N. Kozhevnikov, O. V. Shabunina, V. L. Rusinov and O. N. Chupakhin, *Tetrahedron Lett.*, 2005, **46**, 1791.
17 H.-B. Yu, Q.-S. Hu and L. Pu, *J. Am. Chem. Soc.*, 2000, **122**, 6500.
18 P. F. Schwab, H. F. Fleischer and J. Michl, *J. Org. Chem.*, 2002, **67**, 443.
19 J. J. E. Schmidt, J. A. Krimmel and T. J. Farrell, *J. Org. Chem.*, 1960, **25**, 252.

